Title	Use of bolted steel plates for strengthening of reinforced concrete beams and columns
Author(s)	Su, RKL; Cheng, B; Wang, L; Siu, WH; Zhu, Y
Citation	The IES Journal Part A: Civil And Structural Engineering, 2011, v. 4 n. 2, p. 55-68
Issued Date	2011
URL	http://hdl.handle.net/10722/137224
Rights	This is an electronic version of an article published in The IES Journal Part A: Civil And Structural Engineering, 2011, v. 4 n. 2, p. 55-68. The article is available online at: http://www.tandfonline.com/doi/abs/10.1080/19373260.201156781 6

The Use of Bolted Steel Plates for Strengthening of Reinforced Concrete Beams and Columns

Su RKL[1], Cheng B[1], Wang L[1] , Siu WH[2], Zhu Y[3]

[1] The University of Hong Kong, Hong Kong, China

[2] Ove Arup and Partners Hong Kong Limited, Hong Kong, China

[3] University of Guangzhou, Guangzhou, China

*Corresponding author

Address: Department of Civil Engineering, The University of Hong Kong, Pokfulam Road, Hong Kong, PRC

Fax number: (852) 2559 5337

Tel. number: (852) 2859 2648

E-mail address: klsu@hkucc.hku.hk

Abstract

Reinforced concrete structures often need strengthening due to defective construction, having higher loads than those foreseen in the initial design of the structure, or as a result of material deterioration or accidental damage. The need for strengthening concrete structures has become a crucial problem not only in developed countries but also in China and other developing countries. The use of bolted steel plates to retrofit existing RC structural components has been proven experimentally and practically to be effective in solving the problem. In this paper, experimental and numerical studies conducted at The University of Hong Kong on the strengthening of reinforced concrete coupling beams, floor beams and columns using bolted external steel plates are summarized. Features and design principles of this strengthening method are discussed.

Keywords: bolt slips; bolted steel plate; plate buckling; partial interaction; strengthening.

1. Introduction

Many reinforced concrete (RC) structures require repairs, upgrades or strengthening due to various reasons, such as material deterioration, defective design or construction, structural damage under accidental loads, and change in the functional usage of existing buildings. Three strengthening methods, namely steel jacketing, concrete jacketing and composite jacketing, are commonly adopted for upgrading the load-carrying capacity of RC structures. Among the various strengthening techniques, steel jacketing, which is lightweight, easy to construct, less prone to debonding and has better fire resistance than bonded plates, has been proven to be an effective retrofitting scheme.

In this paper, the experimental and numerical studies conducted at The University of Hong Kong on bolted steel plates retrofitted to RC coupling beams and strengthened RC floor beams and RC columns are reviewed. The major factors affecting the design of this strengthening technique, such as the slips of shear connectors, buckling of steel plates and post-compression effects, are discussed in detail. New structural mechanics models are presented, which allow plate strengthened RC members to be designed with confidence.

2. Shear strengthening of RC coupling beams

2.1 General

Existing RC coupling beams with low shear span ratios and conventionally reinforced shear stirrups tend to fail in a brittle manner with limited ductility and deformability under reversed cyclic loads. To enhance the deformability and energy dissipation of existing RC coupling beams, Su and Zhu (2005), Zhu et al. (2007) and Zhu and Su (2010) proposed a shear strengthening method for RC coupling beams with a span-to-depth ratio of 2.5. Coupling beams were strengthened by bolting the steel plates to two ends of wall panels without adhesive bonding as shown in Figure 1. They conducted experimental and numerical studies to prove that this retrofitting method could greatly increase the shear capacity and deformability of coupling beams subjected to large wind or seismic

loading. Their study also demonstrated that fastening the retrofit plate to the span of RC coupling beam could prevent local buckling of the steel plates but led to serious concrete damage at the failure stage. In all their experiments, minor plate buckling was observed at beam-wall joint regions. Extensive experimental studies and numerical studies were carried out by Su and Cheng (2011), Cheng and Su (2011a and b) on the shear strengthening of deep RC coupling beams with span-to-depth ratios smaller than 2.0, which behave quite differently from medium span coupling beams. They proposed the retrofitting method of laterally restrained side plate (LRSP) as shown in Figure 2. Previous experimental studies (Su and Zhu, 2005, Su and Cheng, 2011 & Cheng and Su, 2011a) on the steel plate strengthened coupling beams showed that unilateral local buckling of steel plates is hard to avoid. Such local buckling usually begins at compressive zones near the beam-wall joints. After buckling, the shear transfer across the beam-wall joints through the steel plate is weakened.

A plate buckling control device, which is composed of steel angles (Figure 2), was suggested to mount to the beam span to suppress plate buckling under shear loads. To avoid adding extra strength and stiffness to the composite coupling beam, the lateral stiffeners are connected to a steel plate by bolt connections with slotted holes, which allow the two lateral stiffeners to freely rotate and move in the longitudinal direction. The advantage of using a plate buckling restraining device instead of adding stiffeners to the steel plates to control plate buckling is that the stiffness of the coupling beams is not increased. Yielding of the plates can be allowed for energy dissipation purposes. It is important because the increase in the beam stiffness would stiffen the lateral load resisting system and cause the structure to attract more seismic loads, which might lead to brittle failure of the coupled shear walls under strong seismic loads. Experimental studies have demonstrated that for the specimens with the added buckling control device, plate buckling at the beam-wall joints was suppressed. A continuous shear transfer medium across the joints that was provided by the steel plate can continue to take a larger share of the load in the post peak region and alleviate concrete crushing in the compression region. As a result, plate strengthened coupling beams failed in a ductile fashion.

Totally eleven coupling beam specimens with span-to-depth ratios (l/h) of 1.1 and 2.5 were previously tested by the The University of Hong Kong. For the specimens with a span-to-depth ratio of 1.1, the sizes of the beams were 450 mm deep by 120 mm wide with a clear span of 500 mm. The top and bottom longitudinal reinforcement in the coupling beams had a steel ratio of 0.84%. For the specimens with a span-to-depth ratio of 2.5, the sizes of the beams were 450 mm deep by 120 mm wide with a clear span of 500 mm. The top and bottom longitudinal reinforcement in the coupling beams had a steel ratio of 1.15%. For both types of specimens, the shear reinforcements consisted of four 8-mm diameter hoops with a 125-mm pitch. This shear reinforcement arrangement was selected to represent the shear-deficient coupling beams in existing buildings. Detailed reinforcement arrangements and bolt-plate configurations can be found in previous experimental studies (Su and Zhu, 2005, Su and Cheng, 2011 & Cheng and Su, 2011a). Specimens CB1 and DCB1 are control specimens without adding steel plates for the shallow and deep beams, respectively.

The material properties of the tested specimens and experimental results are summarised in Table 1. The load-rotation curves of the specimens are shown in Figure 3 (a) and (b) for specimens with span-to-depth ratios of 2.5 and 1.1, respectively. From the test results, it can be concluded that by adding external steel plates, the shear strength can be increased by 40% to 90%, whereas the rotation capacity is increased by 60% to 150%. The increase in the rotation deformability is much higher than the increase in the strength while avoiding increases in the flexural stiffness. The rotation θ_{peak} at peak load may be estimated by the relationship $\theta_{peak} = \alpha\theta_{peak,rc}$, where α ($=V_{max}/ V_{rc}$) is the level of strengthening, and $\theta_{peak,rc}$ and V_{rc} are, respectively, the rotation at the peak load and the shear capacity of the unstrengthened RC coupling beam. The external steel plate retrofitted coupling beams can easily withstand chord rotation demands of 2% and 4% for span-to-depth ratios of 1.1 and 2.5, respectively.

2.2 Estimation of Axial Force

It should be noted that due to the differential longitudinal deformations between the steel plates and concrete beam, an axial compressive force and tensile force are developed in concrete and steel plates, respectively. The ratios of the axial force to shear force of steel plates at the peak loads are shown in Table 1. It is found that such ratios ranged from 0.4 to 1.2. A similar study by Su and Lam (2009) for internal steel plate strengthened coupling beams reveals that this ratio is a function of various parameters, including the plate thickness to beam width ratio, longitudinal steel ratio and span-to-depth ratio of the beam.

Paulay (1971) considered the effects of truss and arch actions in RC coupling beams and proposed the following equation to estimate the beam elongation.

$$\Delta_{lrc} = \frac{V_b l^3}{2A_s E_s z}\left(1 - \frac{V_{sv}}{3V_b}\right) \tag{1}$$

in which V_b and V_{sv} are the shear forces taken by the RC beam and stirrups, respectively, l and z is the span length and moment arm of the beam, respectively, and A_s and E_s are the steel area and Young's modulus of the longitudinal steel, respectively. Considering the horizontal deformation compatibility between the steel plates, bolts and RC beams, the total beam elongation Δ_{lrc} is equal to the sum of the shortening of RC beams, extension of steel plate and the horizontal slip of bolts. By invoking the horizontal force equilibrium, the axial force induced in the steel plate can be estimated by Eq. (2).

$$N_p = \Delta_{lrc} \frac{K_{rc} K_b K_p}{K_p K_b + 2K_p K_{rc} + K_{rc} K_b} \tag{2}$$

and $K_{rc} = \frac{E_c A_c}{l}$, $K_p = \frac{E_p A_p}{l}$, $K_b = n_b K_{b1}$

where K_{rc}, K_p and K_b are, respectively, the axial stiffness of the RC beam and steel plates and the horizontal stiffness of the bolt group at one end of the beam. A_c and E_c are the area and elastic modulus of concrete beam. A_p and E_p are the area and elastic modulus of steel plate. n_b is the number of the anchor bolts at the one end of the beam and K_{b1} is the stiffness of a single bolt

connection. This axial plate force is resisted by the bolt group. Because the axial stress developed in the RC counterpart is usually very small ($\leq 0.1 f_{cu}$), this stress can be neglected in the flexural design of RC beams. For the design of the steel plate, the existence of the axial tensile force is usually beneficial for suppressing the buckling of the steel plate. Further discussions will be given in Section 2.5.

2.3 Anchorage Design

Previous Experimental studies by Su and Cheng (2011) and Cheng and Su (2011a) demonstrated that strong anchorage is beneficial to the energy dissipation ability of the coupling beams especially in the large ductility levels. Strong anchorage can ensure the yielding of plate, which is effective in energy dissipation. For design purposes, the classical elastic theory is introduced for analysing bolt groups subjected to in-plane loads.

Figure 4 shows a general arrangement of a group of bolts subjected to a general external load (F_x, F_y, F_θ).The applied forces at the stiffness centre of the bolt group can be related to the applied forces at the beam-wall joint by Eq.(3).

$$(F_x, F_y, F_\theta) = (N_p, V_p, M_p + V_p(l_{pg} - l/2)). \quad (3)$$

where l_{bg} is the distance from the centre of the bolt group to mid span of the beam, N_p, V_p and M_p is the axial force, shear force and moment induced in the steel plate respectively.

Given that the lateral stiffness of the i^{th} bolt in the x and y directions are k_{xi} and k_{yi}, respectively, and the lateral movements of the bolt group at the stiffness centre are denoted by (Δ_{sl}, Δ_{sv}, θ_{sr}), the slips of the bolt group can be determined based on the classical elastic theory (Su and Siu, 2007) as

$$\begin{Bmatrix} \Delta_{sl} \\ \Delta_{sv} \\ \theta_{sr} \end{Bmatrix} = \frac{1}{-R_x^2 K_y - R_y^2 K_x + I_{zz} K_x K_y} \begin{bmatrix} I_{zz}K_y - R_y^2 & -R_x R_y & R_x K_y \\ -R_x R_y & I_{zz}K_x - R_x^2 & -R_y K_x \\ R_x K_y & -R_y K_x & K_x K_y \end{bmatrix} \begin{Bmatrix} F_x \\ F_y \\ F_\theta \end{Bmatrix} \quad (4)$$

where $K_x = \sum_i k_{x\,i}$, $K_y = \sum_i k_{y\,i}$, $I_{z\,z} = \sum_i \left(k_x y_i^2 + k_y x_i^2\right)$,

$R_x = \sum_i k_{x\,i} y_i$ and $R_y = \sum_i k_{y\,i} x_i$ (5)

After obtaining the slips of the bolt group, the forces at the i^{th} bolt can be calculated by using Eq. (6).

$$\begin{Bmatrix} P_x \\ P_y \end{Bmatrix}_i = \begin{bmatrix} k_{x\,i} & 0 & -k_{x\,i} y_i \\ 0 & k_{y\,i} & k_{y\,i} x_i \end{bmatrix} \begin{Bmatrix} \Delta_{s\,l} \\ \Delta_{s\,v} \\ \theta_{s\,r} \end{Bmatrix} \tag{6}$$

Since the steel plates are attached to coupling beams solely by bolt connections, the properties of the connections can significantly influence the behaviour of the entire retrofitting system. To allow for construction tolerances, clearance through-holes should be provided in the steel plates and concrete walls. Using the special washers (e.g., the dynamic set washer, a proprietary product of HILTI Company Ltd), the gaps between the bolt shank and the surrounding concrete can be filled by injecting adhesive to minimise any bolt-slip between various components at the connections. Figure 5 shows the details of the bolt connection. The advantage of this kind bolt connection is that bolt-slip can be minimized. The load-slip relationship of bolt connections has to be determined with bolt shear tests. To avoid plate buckling in the anchor regions, thicker steel plates in the anchor regions may be used.

2.4 Rotation Compatibility of Retrofitted Coupling Beam

Slips of mechanical connectors in steel plate RC structures can significantly affect the load-carrying capacity of the structures. The difference in deformations between the steel plate and the RC counterpart is known as partial interaction (Oehlers et al., 1997). Figure 6 illustrates the deformation relationships between the RC beam, steel plate and slippage of bolts. By comparing the initial and displaced locations of the stiffness centre of the bolt group, the slips of anchor bolts can be found. In the subsequent discussion, the slips in the longitudinal, transverse and rotation directions are denoted respectively as Δ_{sl}, Δ_{sv} and θ_{sr}. By considering the rotation compatibility between the steel plate and the concrete beam, the total chord rotation θ_t of the plate can be expressed as Eq. (7).

$$\theta_t = \theta_s + \theta_{s\,v} + \theta_{s\,p} + \theta_{s\,i} \tag{7}$$

where θ_s is the rotation due to the change in the reference position from the beam-wall joint to the stiffness centre of the bolt group, θ_{sv} is the rotation caused by the transverse slip of bolts, and θ_p is the combined flexural and shear rotation of the steel plate. Because the longitudinal slip gives only a very small contribution to the rotation compatibility, its effect is neglected in the formulation of Eq.(7). According to Figure 4(b), the rotations θ_s and θ_{sv} can be derived as follows.

$$\theta_s = \theta_{rc}\left(1 - \frac{l}{2l_{bg}}\right) \tag{8}$$

$$\theta_{sv} = \Delta_{sv} / l_{bg} \tag{9}$$

where θ_{rc} is the chord rotation of the RC beam.

Based on Timoshenko's beam theory, the plate rotation due to combined bending and shear can be estimated by Eq. (6).

$$\theta_p = \frac{V_p l_{bg}^2\left[1 + 0.6(1+\nu)\left(\frac{h_p}{l_{bg}}\right)^2\right]}{3E_p I_p} \tag{10}$$

where ν, E_p, I_p and h_p are, respectively, the Poisson's ratio, Young's modulus, second moment of area and depth of the steel plates and V_p is the shear force in the steel plates.

Using Eq.(2) to (4), the rotation components of Specimens CB5 and DCB5 at the peak loads were calculated, and the results are presented in Table 2. It is found that the rotation slip θ_{sr} makes a significant contribution to the total rotation, which implies that to ensure a good composite action between the steel plates and concrete, the rotation slip of the bolt group should be properly controlled. Furthermore, θ_s also significantly affects the total rotation, particularly for deep coupling beams (e.g., Unit DCB5). To enhance the effectiveness of this strengthening scheme, the stiffness centre of the bolt group should be set as close as possible to the beam-wall joint.

Making use of Eqs.(7) to (10), the total rotation due to the slips of the bolt group and the deformation of the steel plates can be obtained.

Using Eq.(7), the total rotations were evaluated and compared with the measured chord rotations of the RC beams in Table 2. The good agreement between the two rotations verified the formulations

of Eqs.(7) to (10). To ensure sufficient stiffness of the bolt group, the total rotation estimated by Eq.(7) is recommended to be not more than (1.2~1.5)× θ_{rc}.

2.5 Effects of Unilateral Plate-buckling

If the strengthening plate is not properly restrained, local buckling, as shown in Figure 7 (a), can occur at the beam-wall regions. The post-peak behaviours including energy dissipation ability and deformability of the retrofitted beams can be adversely affected. Comprehensive experimental studies (Cheng and Su, 2011a) were conducted to examine the effectiveness of providing lateral restraints to control plate buckling. Shear buckling occurred in the span (as shown in Figure 7 (b)) indicated the desired plastic shear deformation. Using the laterally restrained steel plate, the retrofitted coupling beams can achieve better energy dissipation ability and deformability. The ratio of the applied tensile force to the shear force $\beta=N_p/V_p$ was defined to represent the relative intensity between the tensile and shear forces. The effect of the tension field action on the shear carrying of the steel plate under different applied load ratios (β) and different plate thicknesses (t_p) was quantified numerically (Cheng and Su, 2011b).

The finite element package ABAQUS 6.8 was used to perform the simulation of plate buckling with and without a buckling controlled device. Figure 8(a) shows the geometry of the steel plate and the finite element mesh considered in this study. The yield stress of the steel plate was 360 MPa, the Young's modulus was 200 GPa, and the Poisson's ratio was 0.3. To simulate the lateral restraints provided, the lateral movements along the peripheral of the steel plate were restricted. As the stress distribution along the force boundary was not known a priori, transition elements with a larger elastic modulus and yield strength were adopted to distribute the applied loads to the steel plate.

The ultimate moments, M_e and M_o, that respectively correspond to the cases with and without plate buckling were determined. The equivalent ultimate tensile strength of the steel plate σ_e, which is defined in Eq.(11), was then calculated.

$$\sigma_e = \frac{M_e}{M_o}\sigma_o \quad (11)$$

where σ_o is the ultimate tensile stress of the steel plate. Figure 8(b) shows the effects of the force ratio β on the equivalent ultimate tensile stress σ_e of the steel plates. It was found that the presence of a tensile force (i.e., β>0) and the increase in the plate thickness can alleviate local plate buckling and increase the equivalent ultimate tensile stress. When the plate thickness is higher than 6 mm and β is larger than 1, the equivalent ultimate tensile stress is almost the same as the ultimate tensile stress of the steel plate, which implies that under a large tension field, the effect of the geometric nonlinearity vanishes, and the ultimate plate moments (calculated for the cases with and without plate buckling) are the same. For other cases, the effect of plate bucking cannot be ignored, and the ultimate plate moment is reduced.

The case without lateral restraints along the top and bottom edges was also considered in this study. The equivalent ultimate stress is presented as a dotted line in Figure 8(b). The result indicates that the lateral restraints are very effective in increasing the equivalent ultimate stress. Without the restraints, the stress can decrease significantly, in particular when the force ratio β is less than one. The numerical results confirm the importance of providing lateral restraints to the retrofitting steel plates. Because the degree of reduction in the ultimate moment is proportional to the ratio σ_e/σ_o, the tensile strength of the steel plate should be reduced accordingly to account for the plate buckling effect when design the steel plate. From Table 1, the force ratio may be conservatively estimated to be around 0.45. For thin steel plates (e.g., 3 mm in thickness), the reduction of shear strength due to plate buckling can be as high as 15%.

A finite element analysis was conducted to predict the ultimate strength of laterally restrained steel plates. The analysis studied 36 steel plates with different configurations: the plate span (l_p) of 500mm, 1000mm or 2000mm, the span-to-depth ratio (l_p/h_p) of 1.0, 1.5, 2.0 or 2.5, and the plate slenderness ratio (h_p/t_p) of 62.5, 100 or 166. Based on the numerical results, the design model for the equivalent yield stress of steel plate was proposed as shown in Figure 9. The results presented

may be used by the engineer for estimating the ultimate shear or flexural capacity of laterally restrained steel plates.

3. Flexural strengthening of RC floor beams

3.1 General

Existing RC beams can be strengthened with externally bolted side plates (see Figure 10). Compared with other strengthening schemes, the use of bolted side plates can maintain the ductility of the beam, prevent the anchor bolts from clashing with the main bottom steel bars and free up the bottom surface to facilitate the installation of props below the beam during strengthening construction. However, the flexural strength and stiffness of this type of bolted side-plate beam can be affected by the partial interaction between the steel plates and RC beams due to the mechanical slip of bolts. To avoid over-estimation of the flexural strength and to ensure accurate prediction of the load-deformation response of the beams, the effect of partial interaction has to be properly considered.

A detailed experimental study (Siu and Su, 2010 and Siu, 2009) using four-point bending tests was carried out to investigate the effects of bolt-plate arrangements and partial interaction on bolted side-plated beams. Five specimens were fabricated and tested. The dimensions of the RC beams were 225×350×4000 mm (width×depth×length); and the beams were simply-supported with a clear span of 3600 mm. The beams were under-reinforced by 3T16 longitudinal reinforcements. Transverse reinforcement of T10-150 was applied throughout the span of the beams. This amount of reinforcement causes the specimens to fail in flexure in both the un-strengthened and strengthened cases.

Specimen NBNP is the control specimen without any strengthening measures. The other specimens are plate strengthened with four different bolt-plate combinations including ‘strong-bolt strong-plate’ (SBSP), ‘weak-bolt strong-plate’ (WBSP), ‘weak-bolt weak-plate’ (WBWP) and ‘strong-bolt weak-plate’ (SBWP).

The strengthening details are summarised in Table 3. Mild steel plates of two different plate sizes, 6×150 mm deep and 6×75 mm deep, on both side faces of specimens were chosen to be the 'strong' and 'weak' plate arrangements, respectively. The centroidal axes (h_p) of the steel plates in all strengthened specimens were set at 250 mm from the top of the beam. By setting the centroidal axis to a level on the tension side and relatively further away from the neutral axis, the buckling of steel plates is prevented. Detailed arrangements of reinforcement and anchor bolts as well as their material properties can be found in Siu (2009).

The ultimate strengths and failure modes of the five specimens are presented in Table 3; and the moment-deflection responses at the mid-span of the five specimens are plotted in Figure 10. The ultimate strength of BSP specimens was increased by 32% to 59% to the ultimate capacity of the unstrengthened specimen NBNP. Specimen SBSP, strengthened by both a 'strong bolt' and 'strong plate', was the strongest among the specimens.

Two different failure modes were observed for 'strong' bolt and 'weak' bolt specimens. Specimens (SBSP and SBWP), with sufficient bolts installed, failed in concrete crushing after the yielding of the bottom reinforcement. Specimens (WBSP and WBWP), with insufficient bolts installed, failed in bolt fracture. In both specimens, the bolts closest to the supports fractured, leading to an abrupt failure.

As shown in Figure 11, the responses of 'strong' bolt and 'weak' bolt specimens are quite different. The response of 'strong' bolt specimens (SBSP and SBWP) is better. After the initial linear deformation against the applied load, the stiffness dropped gradually, but the specimens were still able to take up further loading up to the peak load. After reaching the peak load, a gradual descending branch was observed due to crushing of concrete until failure occurred.

The displacement ductility factors of beam specimens are given in Table 3. The displacement ductility of all plate strengthened beams were lower than the un-strengthened beam as expected because the bolt-plate system acts as an additional reinforcement to the beam and hence reduces the displacement ductility of the bolted side plate beams.

From the displacement ductility factor and the degree of strengthening, it is found that combining the use of ‘Strong bolts’ with a limited amount of steel plates can effectively enhance the post-elastic strength of beam with a satisfactory level of ductility, meaning that ‘strong-bolt weak-plate’ arrangement is the safer strengthening system because the post-elastic branch provides a warning signal to occupants if the structure is overloaded prior to collapse. However, the ‘strong-bolt strong-plate’ arrangement results in a brittle and undesirable failure, which suggests that the amount of steel plates added should be limited, whereas sufficient bolts should be used to ensure the beam failure is in a desirable ductile mode.

3.2 Effects of partial interaction

Both transverse and longitudinal partial interactions exist in the strengthened beam, which leads to a separation of strain profiles for RC and the strengthening plates, thus reducing the force and moment induced in the plates and eventually the flexural strength of bolted side-plate beams. The maximum slips at peak loads at the supports of all specimens are summarised in Table 3, and the longitudinal slip responses of Specimens SBWP and WBSP are plotted in Figure 12. The responses between ‘strong’ bolt and ‘weak’ bolt specimens are significantly different. For the ‘strong’ bolt specimens (e.g., SBWP), the slips were very small (<0.2 mm) when initial loading was applied because most of the force transferred to the steel plates was taken up by the friction between the RC beam and the steel plates. The bolts were mobilised as the applied load increased, and the longitudinal slips at various locations along beam span and the mid-span deflections was proportionally increased until the mid-span deflections reached the deflections corresponding to the peak load. In the post-peak stage, the slips increased more slowly than in the pre-peak stage, until failure occurred. All the ‘weak’ bolt specimens (e.g., WBSP) failed in bolt fracture. The ductility demand for bolts is much higher than that for the beam. Bolts with very high deformability should be used when adopting ’weak’ bolt arrangements in practical designs.

Two parameters, the strain factor and the curvature factor, as illustrated in Figure 13(a), were proposed to quantify the partial interaction at the peak moment section. These two factors quantified the ratio of cross-sectional deformation between the RC beam and the steel plates and are able to describe the interaction between the RC beam, the steel plate and the anchoring bolts.

The longitudinal partial interaction is quantified by the strain factor of the critical section, which is defined mathematically as

$$\alpha_{\varepsilon} = \frac{\varepsilon_{p,h_p}}{\varepsilon_{c,h_p}} \tag{12}$$

where $\varepsilon_{p,hp}$ and $\varepsilon_{c,hp}$ are the longitudinal strains of the steel plates and the RC beam at the centroidal level of the steel plate of the corresponding section, respectively. When the strain factor is equal to 1, full longitudinal partial interaction exists, and the longitudinal strain at the centroidal level of the plate is the same as that of the adjacent concrete. In this case, the maximum plate force is induced in the steel plates. When partial interaction exists, the strain factor is smaller than 1, and the longitudinal strain is reduced to $\alpha_{\varepsilon}\varepsilon_{c,hp}$. In the extreme case, the strain factor is zero, and no net axial force is induced in the steel plates. Considering the compatibility between the RC beam, the steel plates and slip at the critical section, as shown in Figure 13(a), the strain in concrete, and hence the strain factor, can be expressed in terms of the strain in the steel plates and the slip strains at the centroidal level of the steel plates as

$$\varepsilon_{c,h_p} = \varepsilon_{p,h_p} + \varepsilon_{slip,h_p}, \tag{13}$$

$$\alpha_{\varepsilon} = \frac{\varepsilon_{p,h_p}}{\varepsilon_{p,h_p} + \varepsilon_{slip,h_p}}. \tag{14}$$

On the other hand, the curvature factor of the critical section is used to quantify the transverse interaction between the RC beam and the steel plate and is defined as

$$\alpha_{\phi} = \frac{\phi_p}{\phi_c} \tag{15}$$

where ϕ_p and ϕ_c are the curvatures of the steel plates and the RC beam of the corresponding section, respectively. Full transverse interaction is present when the curvature is equal to 1 and the curvatures of the RC beam and the steel plates are the same. When partial interaction exists, the

curvature of the steel plates is smaller than that of the RC beam, and the curvature factor is between 0 and 1. When the curvature factor is 0, the beam exhibits no transverse interaction. The typical variations of the strain factor and curvature factor against the mid-span deflection for Specimen SBWP are shown in Figure 13(b). A gradual descending trend for the strain factor is observed. The gradual drop in strain factor is mainly due to the non-linear load-slip response caused by the stiffness reduction of anchor bolts. This results in a reduction of the longitudinal partial interaction of the beam.

A significant drop in strain factor implies that the strain in the steel plate is much lower than the strain in the adjacent concrete, at the centroidal level of the steel plate. The strain reduction in the steel plates reduces the chance of plate yielding, and can greatly reduce the moment capacity of the strengthened beam. The low chance of plate yielding at the peak moment implies that assuming the steel plates to be plastic at the ultimate state, as adopted in rigid plastic analysis, may not be correct, and the strength of the beams can be over-estimated if the steel plate is assumed to be plastic. When more bolts are used, the stiffness of the connecting media is increased. A smaller slip of bolts is enough for developing the same amount of axial plate force. Thus, the slip strain will be decreased, resulting in a larger strain factor (see Eq. (14)).

The curvature factor is larger than 0.9 prior to yielding of the bottom reinforcement, which means that the difference in curvatures between the RC beam and steel plate at the critical section is small and that there is a strong transverse interaction between the RC beam and the steel plates in the elastic stage. Unlike the variation of strain factor in the elastic stage, the curvature remains almost constant throughout the elastic stage, which suggests that the transverse partial interaction response is less sensitive to the gradual drop in bolt stiffness, as compared with the longitudinal partial interaction response.

After yielding of the bottom reinforcement, the curvature factors begin to drop gradually. The reduction in curvature can be explained by the formation of plastic hinges at the critical section. When a plastic hinge forms in the RC beam, the flexural stiffness of the plastic hinge zone drops to

almost zero and thus the curvature of the RC beam increases dramatically when deformed further. On the contrary, due to the reduction of strain in the steel plates, a plastic hinge is unlikely to form in the steel plates, and thus the curvature in the steel plates will not increase as quickly as that of the RC beam. Both effects, together, resulted in the decreasing trend of curvature factor.

3.3 Strain and curvature factors

Using the Euler's beam theory, the general forms of the strain factor and curvature factors can be derived. The strain factor can be expressed as

$$\alpha_{\varepsilon} = \frac{1}{1 + \frac{-s_l'(L_s)(EA)_p}{\int_0^{L_s} k_m(x) s_l(x) dx}} \tag{16}$$

where $(EA)_p$ is the product of the Young's modulus and the sectional area of the steel plate, k_m is the stiffness of the media of connection per unit length, L_s is the span length from zero moment to maximum moment, $s_l(x)$ is the longitudinal slip profile along the beam span, and $s_l'(L_s)$ is the slope of the slip profile at the location of the maximum moment. The strain factor is readily solved once the longitudinal slip profile along the span is available. It is noted that the expression $s_l'(L_s)(EA)_p / \int_0^{L_s} k_m(x) s_l(x) dx$ ranges from 0 to $+\infty$. When it is equal to zero, the strain factor becomes one, and full interaction exists. On the contrary, when the expression approaches infinity, the stiffness of the connecting media k_m approaches zero, and the strain factor becomes zero; there is no interaction between the steel plates and concrete beam.

The curvature factor can be expressed as

$$\alpha_{\phi} = \frac{1}{1 + \frac{(EI)_p}{k_m} \frac{s_v''(x)}{\int_0^{L_s} \int_0^{L_s} k_m s_v(x) dx \, dx}} \tag{17}$$

where $(EI)_p$ is the product of the Young's modulus and the second moment of area of the steel plate, $s_v(x)$ is the transverse slip profile, and $s_v''(x)$ is the second derivative of the transverse slip profile

with respect to the space coordinate *x*. This factor can be solved once the transverse slip profile and the geometry of the beam are defined. The experimental results (Siu, 2009) indicate that the curvature factor remains a constant (from 0.9 to 1) before reaching the peak load.

Using Eqs.(16) and (17), the global partial interaction problem can be transformed into a local sectional analysis, and then the moment resistance of the section can be obtained. Obviously, the moment capacity of bolted side plate RC beams is governed by these two factors.

The strain and curvature factors as well as the corresponding slip profiles of some simple loading cases have been determined (Siu and Su, 2009 and 2011). However, for complicated loading and support conditions, the analysis has to be conducted numerically.

4. Axial strengthening of RC columns

4.1 General

A simple and innovative post-compression approach was proposed by Su and Wang (2009) to strengthen preloaded RC rectangular columns. In this approach, precambered steel plates are bolted to the RC column (see Figure 14a). Because the plates provided are longer than the clear height of the column, progressive tightening the anchor bolts can generate a thrust on the beam supports by means of arching actions. Unlike other reinforcement methods, the present approach can actively share the existing axial loads in the original column with additional steel plates. The stress relief in the original column and post-stress developed in the steel plates can alleviate the stress lagging and displacement incompatibility problems. Because similar strains are induced in the RC column and steel plates, a better utilisation of both components in resisting external loads and a higher axial load-carrying capacity can be achieved.

The theory of this reinforcement method is similar to the principle of pre-stressed concrete. The amount of post-compressed plate forces induced is controlled by the initial precamber of the pre-cambered plates. By applying this reinforcement method in each floor successively, the additional

loads can be transferred down to the foundation (see Figure 14b). To ensure reliable transmission of the load through the floor diaphragm, capitals or steel tubes might be added to the ends of the steel plates.

4.2 Estimation of Axial Force

Due to the fact that bolts at both ends of the steel plates restrain the end rotations of plates, the initial lateral displacement (v) of the precambered plate can be approximated by a cosine function as expressed in Eq. (18).

$$v = \frac{\delta}{2}\left(1-\cos\left(\frac{2\pi x}{L_{rc,pl}}\right)\right) \tag{18}$$

where δ is the initial precamber at the mid-height of the plate, $L_{rc,pl}$ is the clear height of the RC column under preloading (N_{pl}), x is the coordinate defined along the height of the column, and the subscript *pl* denotes the preloading stage. Eq. (18) satisfies the boundary conditions at both ends of the steel plates, i.e., $v = 0$ and $\frac{dv}{dx} = 0$ when $x = 0$ or $x = L_{rc,pl}$.

Based on the principles of force equilibrium and displacement compatibility, the theoretical ultimate axial load capacity of plate-strengthened RC columns can be expressed as

$$N_{prc} = 0.67A_c f_{cu} + A_s f_{sy} + 2\gamma A_p f_{py} \tag{19}$$

where f_{cu}, f_{sy} and f_{py} are concrete cube compressive strength, yield strength of the steel bar and yield strength of steel plate, respectively. A_c, A_s and A_p are cross-sectional areas of the RC column, vertical steel bars and a steel plate, respectively. γ is defined as plate strength utilisation coefficient, which can be expressed as Eq.(20).

$$\gamma = \begin{cases} \dfrac{E_p\varepsilon_{c0}\left(-5E_sA_s\varepsilon_{c0}+\sqrt{A_c f_{cu}\left(64A_c f_{cu}+80E_sA_s\varepsilon_{c0}+160E_pA_p\varepsilon_{p,ps}-80N_{pl}\right)+25E_s^2A_s^2\varepsilon_{c0}^2}\right)}{8A_c f_{cu} f_{py}} & (\varepsilon_p < \varepsilon_{py}) \\ 1 & (\varepsilon_p \geq \varepsilon_{py}) \end{cases} \tag{20}$$

where E_s and E_p are Young's modulus of steel bar and plate, respectively. ε_{co} is the concrete compressive strain corresponding to f_c', which is the concrete cylinder compressive strength, usually equal to 0.8 of the concrete cube compressive strength (f_{cu}). $\varepsilon_{p,ps}$ is the axial strain in the steel plates in the post-stressing stage. ε_{py} is yield strain of steel plate.

The coefficient 0.67 is used to account for a number of factors involving the height-to-width ratio of the RC column, the loading rate and the compaction of concrete was proposed by Kong *et al*. (1987). This value has been widely adopted by various researchers; for instance, by Park and Paulay (1975).

If the local buckling of steel plates occurs before the plate-strengthened column reaches its ultimate load capacity, then the critical load of the steel plate ($N_{p,cr}$) can be calculated by the Euler equation Timoshenko (1961).

$$N_{p,cr} = \frac{\pi^2 E_p I_p}{(\mu s_{\max})^2} \tag{21}$$

where s_{max} is the maximum bolt spacing and μ is a factor related to the boundary conditions for the columns. In the present case, as both ends of the steel plates are clamped, μ is equal to 0.5.

To prevent local buckling of the steel plates, the plate buckling load should be higher than the designed axial force in the steel plate. Hence,

$$N_{p,cr} > \gamma A_p f_{py} \tag{22}$$

The maximum bolt spacing for preventing local plate buckling can be determined by using Eqs. (21) and (22).

4.3 Post stressed procedure

One of the key steps in this strengthening method is to decompress the RC column by flattening the precambered steel plates. A major difficulty is that the steel plates could be warped (buckled) if the post-stress procedure is not conducted properly. This could alter the effectiveness of the decompression process.

To overcome this difficulty, a unified post-stress procedure is proposed, as shown in Figure 15. In order to increase the critical buckling load of plates and to avoid warping effects, precambered plates were pressed to form high-order buckling modes, instead of a first-order buckling mode, during the post-stress procedure. The process can be divided into the following three steps: (i) bolts at the mid-height are tightened as shown in Figure 15(b); thus, the buckling mode of the precambered plate is changed to higher modes, (ii) the plates are flattened by tightening the other bolts as shown in Figure 15(c) and (iii) to achieve a more evenly distributed internal stress in the plates, all the bolts are slightly loosened and fastened again as shown in Figures 15(d) and (e).

4.4 Specimens and ultimate axial load capacity

Four specimens, namely SC1, SC5, SC7 and SC8 were fabricated and tested. The RC details of all specimens are identical. The RC cross sections were 100mm×150mm and the clear heights of columns were 600mm. The vertical reinforcement of 4T10 was arranged and transverse reinforcement of R6-80 was applied throughout the height of the column.

Specimen SC1 was a control column without any strengthening measure. It was used to demonstrate the structural performance of the RC column specimen prior to strengthening. Another three specimens were strengthened by precambered steel plates. The steel plates were fixed by Grade 8.8 bolts of diameter 12 mm. Slight larger clearance holes of 16 mm diameter were provided for tolerances in fabrication and drilling of holes in the steel plates. The structural glue, produced by HILTI Co., Ltd., was injected into the top and bottom holes to prevent slippages within the clearance hole. All the experimental data of the specimens and material properties are summarised in Table 4.

The load-deflection curves of four specimens are plotted in Figure16. The plate-strengthened columns behave more ductile than the control column. Comparison to the control column SC1, the ultimate capacity of SC5, SC7 and SC8 were increased by 17.9%, 51.7% and 63.4%, respectively. The experimental axial capacities (P_{exp}) together with the theoretical predictions (P_{theory}) are shown

in Table 4. The good agreement between the experimental and theoretical results validates the proposed theory.

5. Acknowledgements

The research described here was supported by the Research Grants Council of the Hong Kong SAR (Project No. HKU7166/08E).

References

Cheng, B., and Su, R.K.L., 2011a. Retrofit of deep concrete coupling beams by a laterally restrained side plate. Journal of Structural Engineering - American Society of Civil Engineers (Accepted in April 2010)

Cheng, B., and Su, R.K.L., 2011b. Numerical studies of deep concrete coupling beams retrofitted with a laterally restrained steel plate. Journal of Advances in Structural Engineering, (Accepted in Dec 2010)

Hognestad, E., Hanson, N. and Mchenry, D., 1955. Concrete stress distribution in ultimate strength design. ACI Structural Journal, 52(6), 455-479.

Kong, F.K. and Evans, R.H., 1987. Reinforced and prestressed concrete, 3rd, ed. London: Van Nostrand Reinhold (International).

Oehlers, D.J., Nguyen, N.T., Ahmed, M., and Bradford, M.A., 1997. Transverse and longitudinal partial interaction in composite bolted side-plated reinforced-concrete beams. Structural Engineering and Mechanics, 5(5), 553-564.

Park, R, and Paulay, T. 1975. Reinforced concrete structures. John Wiley & Sons publications.

Paulay, T., 1971.Coupling beams of reinforced concrete shear walls. Journal of Structural Division, Proceedings of the American Society of Civil Engineers, 97 (ST3), 843-862.

Su, R.K.L. and Zhu, Y., 2005. Experimental and numerical studies of external steel plate strengthened reinforced concrete coupling beams. Engineering Structures, 27(10), 1537-1550.

Su, R.K.L., and Cheng, B. 2011, Plate strengthened deep reinforced concrete coupling beams. Proceedings of the Institution of Civil Engineers-Structures & Buildings (Accepted in July 2009).

Su, R.K.L., and Lam, W.Y., 2009. A unified design approach for plate-reinforced composite coupling beams. Journal of Constructional Steel Research, 65(3), 675-686.

Su, R.K.L., and Siu, W.H., 2007. Nonlinear response of bolt groups under in-plane loading. Engineering Structures, 29(4), 626-634.

Su, R.K.L., Siu, W.H., and Smith, S.T., 2010. Effects of bolt-plate arrangements on steel plate strengthened reinforced concrete beams, Engineering Structure, 32(6), 1769-1778.

Su, R.K.L., and Wang, L., 2009.Compressed plates for strengthening preloaded rectangular reinforced concrete columns. Proceedings of the 7th International Conference on Tall Buildings, 29-30 October , Hong Kong China, 193-201.

Siu, W.H., 2009. Flexural strengthening of reinforced concrete beams by bolted side steel plates, PhD Thesis, The University Hong Kong, Hong Kong.

Siu, W.H., and Su, R.K.L., 2009. Nonlinear analysis of bolted side-plated reinforced concrete beams. Proceedings of the First International Conference on Computational Technologies in Concrete Structures, 24-27 May, Jeju, Korea, 667-679.

Siu, W.H., and Su, R.K.L.,2010. Effects of plastic hinges on partial interaction behaviour of bolted side-plated beams. Journal of Constructional Steel Research, 66(5), 622-633.

Siu, W.H., and Su, R.K.L. 2011. Analysis of side-plated reinforced concrete beams with partial interaction. Computers and concrete, 8(1), 71-96.

Timoshenko, S.P., Gere, J.M., 1961.Theory of elastic stability. Mcgraw-Hill.

Zhu, Y., and Su, R.K.L. 2010. Behavior of strengthened reinforced concrete coupling beams by bolted steel plates. Part 2: evaluation of theoretical strength. Structural Engineering and Mechanics, 34(5), 563-580.

Zhu Y., Su, R.K.L., and Zhou, F.L., 2007. Seismic Behavior of strengthened reinforced concrete coupling beams by bolted steel plates, part 1: experimental study. Structural Engineering and Mechanics, 27(2), 149-172.

Table 1 Summary of material properties and experimental results of bolted plate RC coupling beams

Unit	f_{cu} (MPa)	t_p (mm)	f_{yp} (MPa)	V_{max} (kN)	v_{max} (MPa)	θ_y (rad)	θ_u (rad)	K_o (kN/mm)	N_p/V_p
l/*h*=2.5									
CB1	50.2	N/A	N/A	213	3.9	0.0078	0.023	38	N/A
CB2	49.1	3	326	291	5.3	0.0095	0.037	40	0.61
CB3	44.3	6	337	363	6.7	0.0129	0.048	37	0.58
CB4	54.4	3	326	354	6.5	0.0117	0.036	41	0.83
CB5	50.7	6	337	418	7.7	0.0158	0.056	35	1.06
l/*h*=1.1									
DCB1	32.8	N/A	N/A	238	4.4	0.0052	0.012	76	N/A
DCB2	35.1	3	359	344	6.4	0.0085	0.019	67	1.16
DCB3*	33.7	3	362	315	5.8	0.0067	0.023	78	1.00
DCB4*	33.1	3	354	346	6.4	0.0072	0.022	80	0.86
DCB5*	33.0	3	330	335	6.2	0.0065	0.022	83	0.43
DCB6*	35.3	4.5	353	356	6.6	0.0067	0.032	88	0.43

Note: f_{cu} = the cube compressive strength of concrete
t_p = the total thickness of steel plates
f_{yp} = the yield stress of steel plates
V_{max} = the maximum shear capacity of the specimen
v_{max} = the maximum shear capacity of the specimen
θ_y = the nominal yield chord rotation of the specimen
θ_u = the ultimate chord rotation of the specimen
K_o = the stiffness of the specimen
V_p= shear force of the plate
N_p= axial force of the plate
* Specimen installed a plate buckling control device

Table 2 Rotation components and chord rotation of beams

Unit	θ_s (rad)	θ_p (rad)	θ_{sv} (rad)	θ_{sr} (rad)	θ_t (rad) from Eq.(7)	θ_{peak} (rad) Exp.
DCB5	0.0035 (39%)	0.0024 (19%)	0.0005 (4%)	0.0048 (38%)	0.0127	0.013
CB5	0.006 (21%)	0.0036 (12%)	0.0020 (7%)	0.0174 (60%)	0.0290	0.0289

Note: The value in the bracket represents the contribution to total rotation in percentage.

Table 3 Summary of bolt-plate arrangements and experimental results of bolted steel plate floor beams

Unit	NBNP	SBSP	WBSP	WBWP	SBWP
No. of bolts on shear span[#]	N/A	8	3	3	5
Plastic strength of bolts on a shear span P_b (kN)	N/A	608	228	228	380
Plate size[#] (mm×mm)	N/A	6×150dp.	6×150dp.	6×75dp.	6×75dp.
Maximum plate force from full interaction analysis $F_{p,fi}$ (kN)	N/A	605	605	302	302
Concrete cube strength (MPa)	35.2	34.6	34.3	35.1	35.3
Failure mode	Concrete crushing	Concrete crushing	bolt fracture	bolt fracture	Concrete crushing
Ultimate moment (kNm)	101.4	161.5	149.2	133.4	144.6
Displacement ductility capacity	3.62	1.70	2.30	2.57	2.45
Bolt slip at supports (mm)	N/A	1.2	4.6	4.2	1.7

#value refers to the plate on each face of the beam

Table 4 Summary of and experimental data of specimens and material properties

Unit	f_{cu} (MPa)	t_p (mm)	*precamber* (mm)	f_{sy} (MPa)	f_{py} (MPa)	γ	P_{exp} (kN)	P_{theory} (kN)	P_{exp}/P_{theory}
SC1	31.3	-	-	480	-	-	549	459	1.20
SC5	31.2	3	10	480	318	0.82	647	609	1.06
SC7	28.5	6	6	480	322	0.68	833	761	1.10
SC8	28.5	6	10	480	322	0.84	897	848	1.06

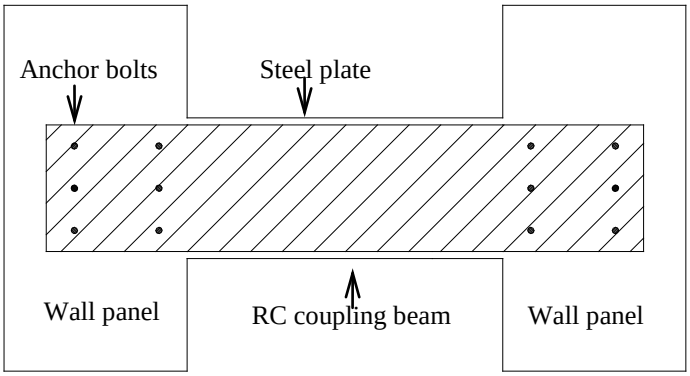

Figure 1 Retrofitting method of bolted steel plate proposed by Su and Zhu (2005)

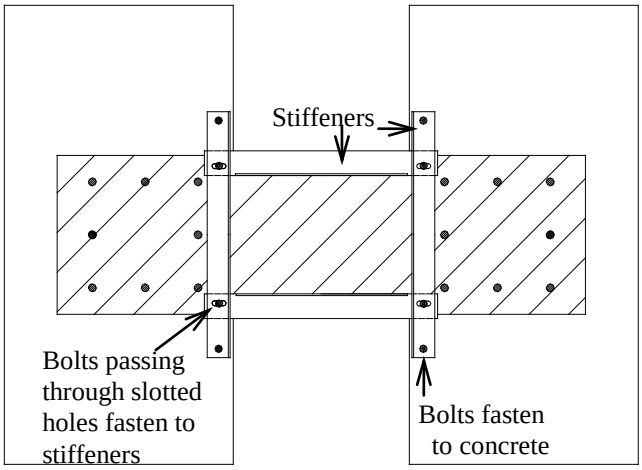

Figure 2 Retrofitting method of laterally restrained side plate proposed by Su and Cheng (2011)

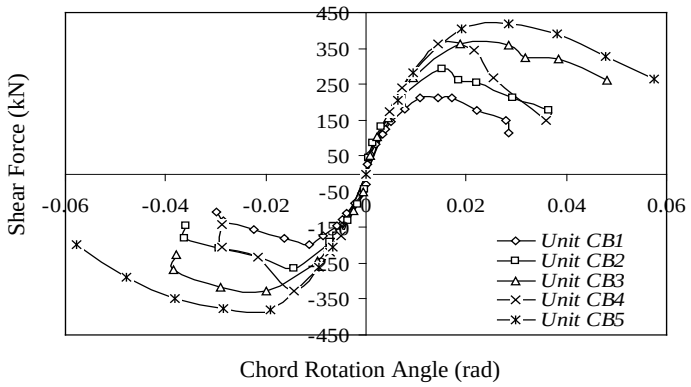

(a)

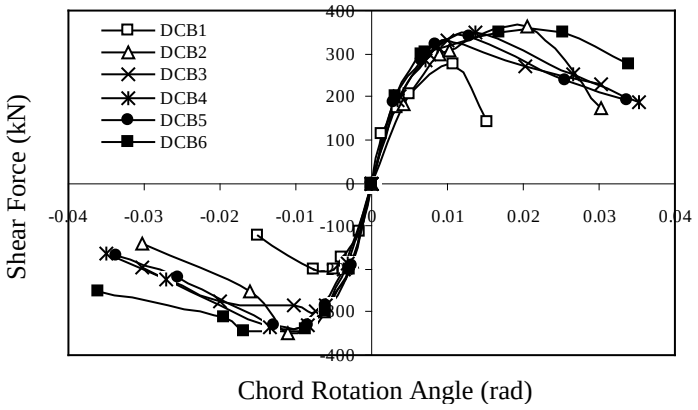

(b)

Figure 3 Envelops of load-rotation curves of specimens (a) *l/h*= 2.5, and (b) *l/h* =1.1

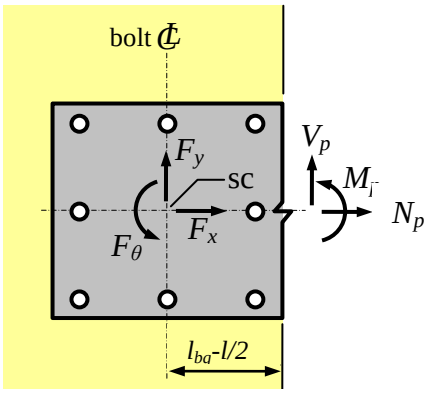

Figure 4 Bolt group and applied forces

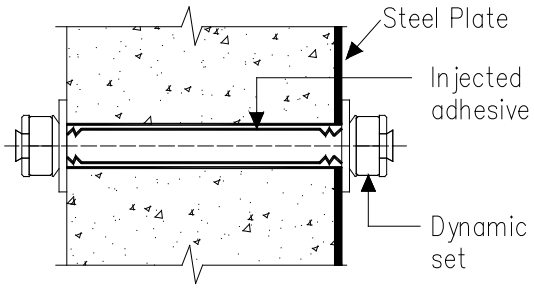

Figure 5 Details of Bolt Connection

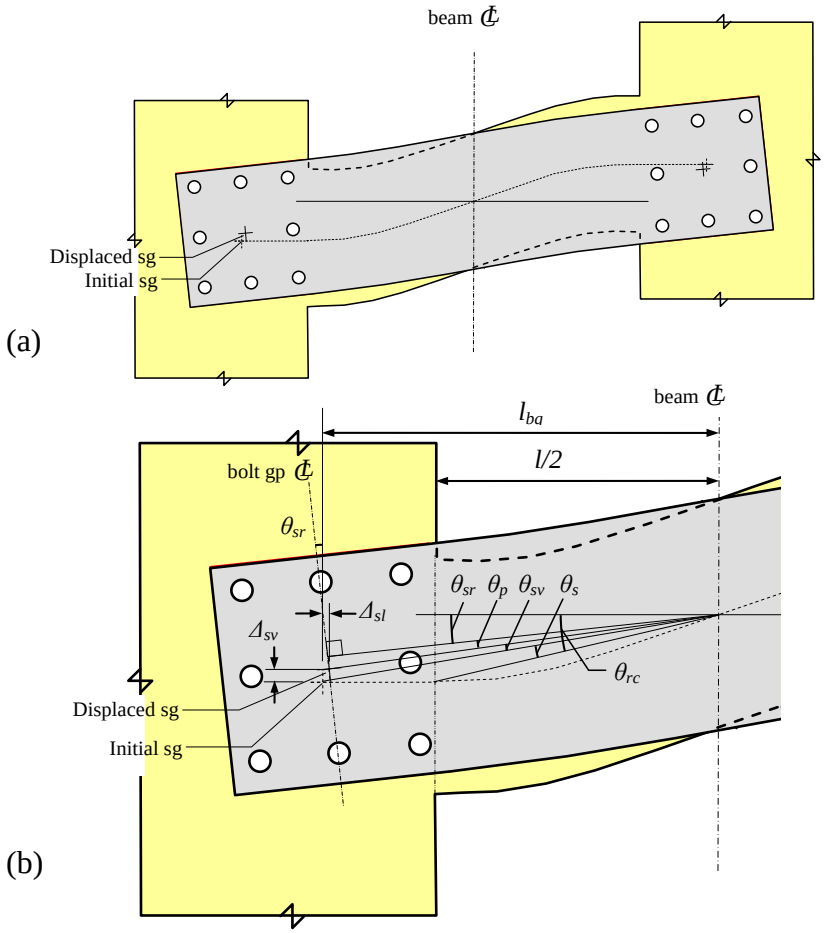

Figure 6 Longitudinal, transverse and rotation slips (a) overall deformations and (b) slip components

(a) CB5 (b) DCB5

Figure 7 Plate buckling of Unit CB5 and Unit DCB5

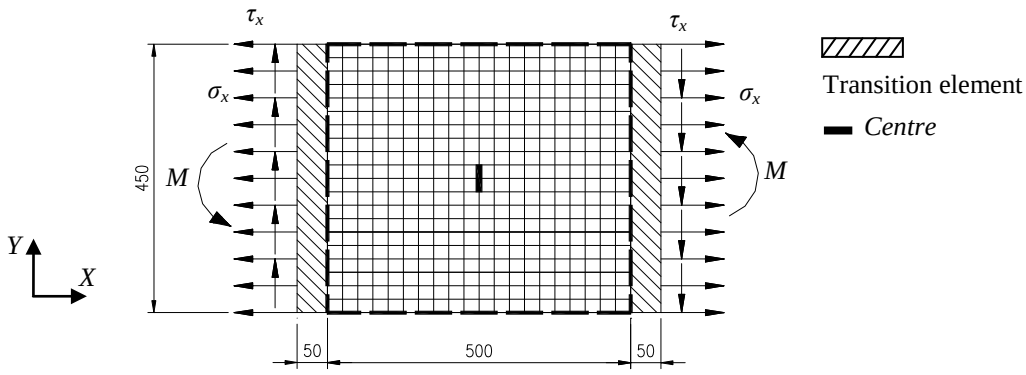

(a)

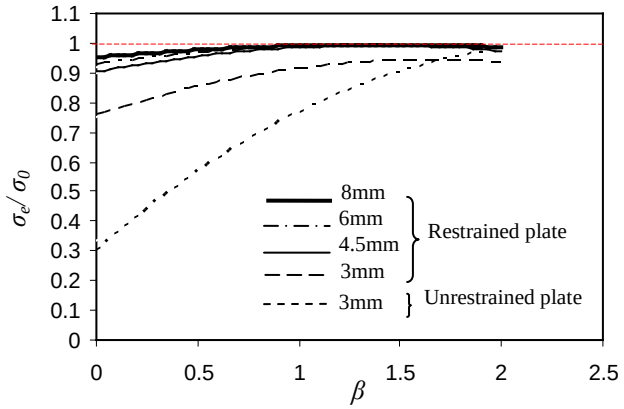

(b)

Figure 8 Effect of the tension field action (a) the finite element mesh, and (b) the equivalent ultimate tensile stress against N_p/V_p

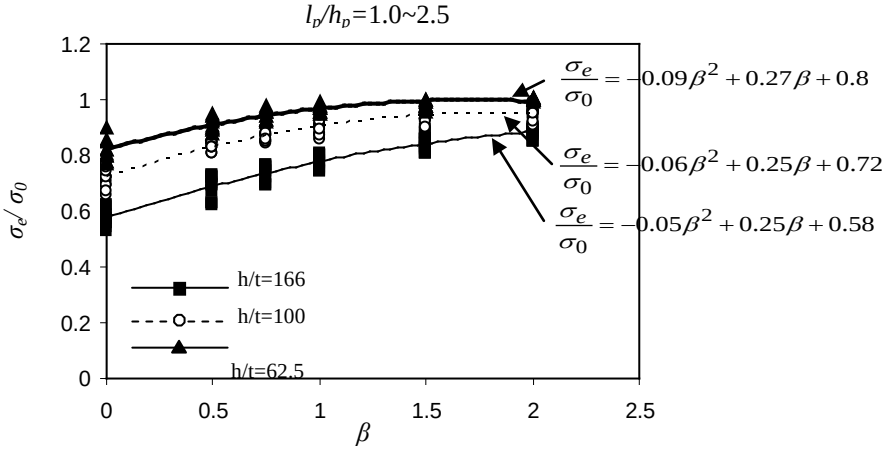

Figure 9 Equivalent Ultimate von-Mises Stress Design Model

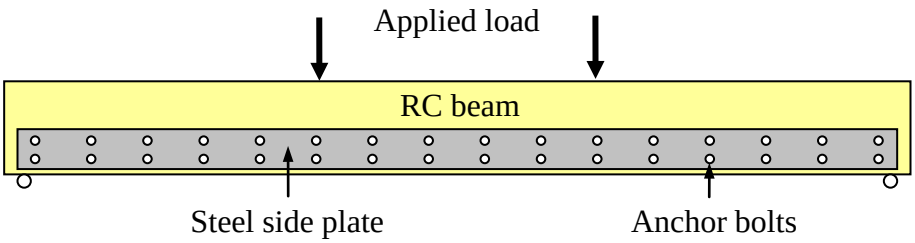

Figure 10 An external steel plate strengthened floor beam

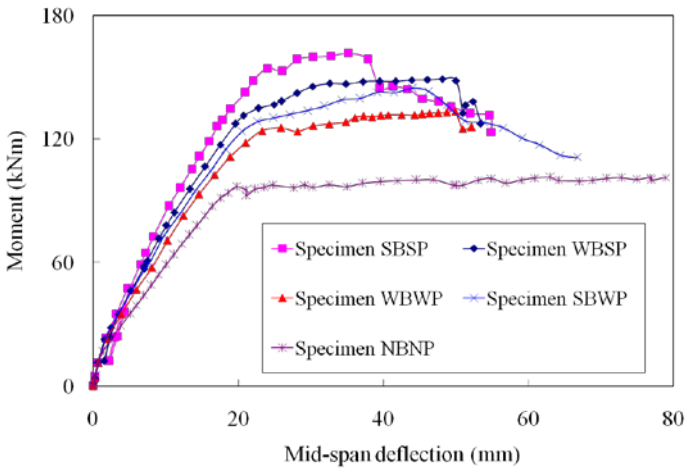

Figure 11 Moment-deflection curves of plate strengthened floor beams

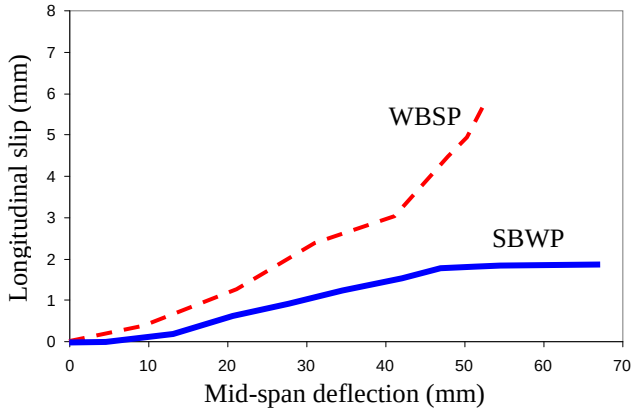

Figure 12 Longitudinal slip responses at supports of Specimens SBWP and WBSP

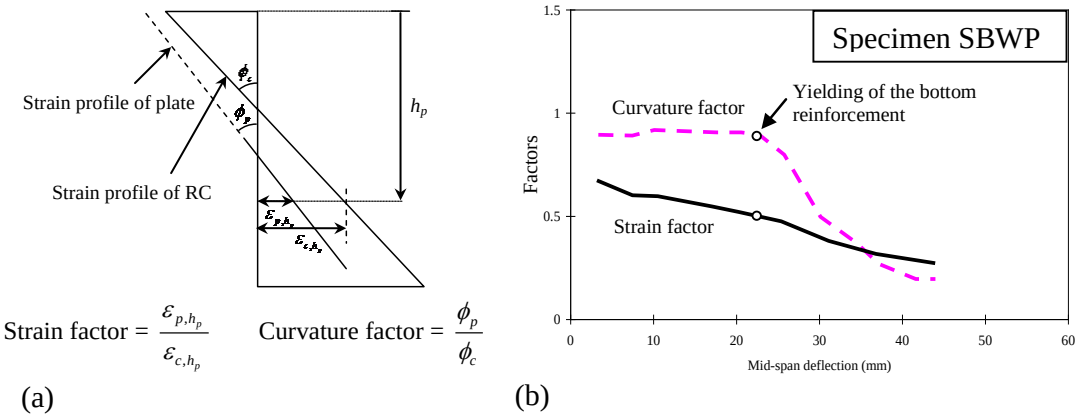

Figure 13 Strain factor and curvature factor (a) definitions and (b) typical variations

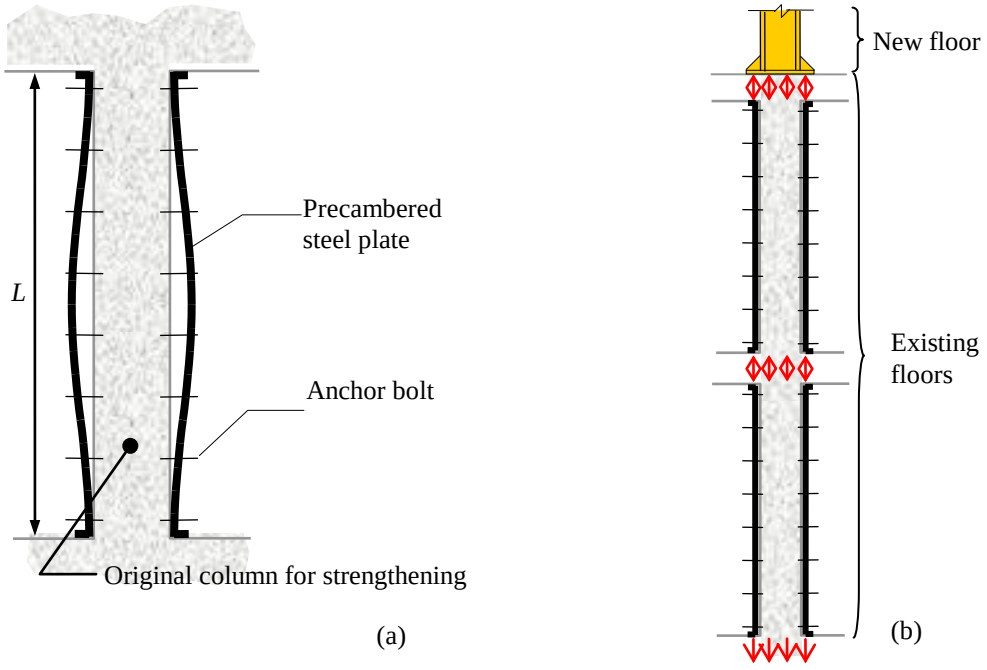

Figure 14 Illustration of column strengthening by post-compression plate for (a) single storey, and (b) multiple storeys

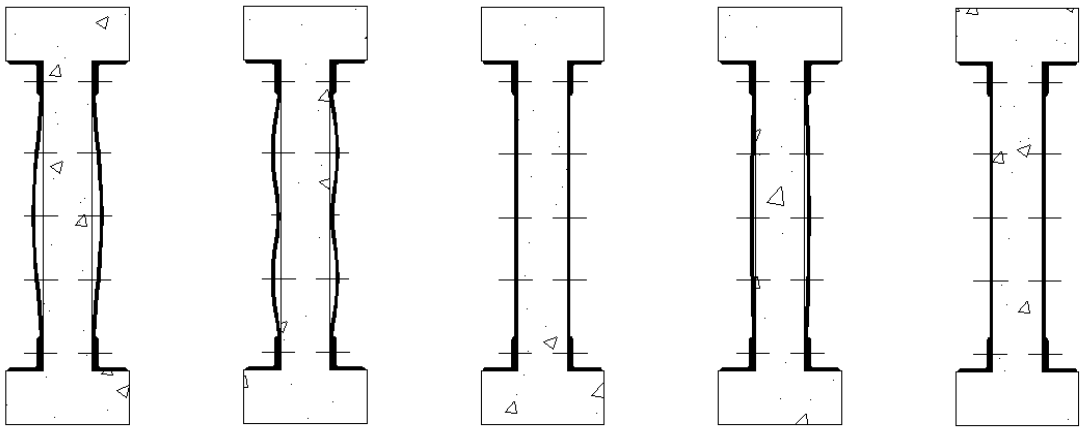

(i) Initial state | (ii) Tightening the mid-height bolts | (iii) Flattening the plates | (iv) Loosening the bolts | (v) Fastening the bolts again

Figure 15 Post-stressed procedure

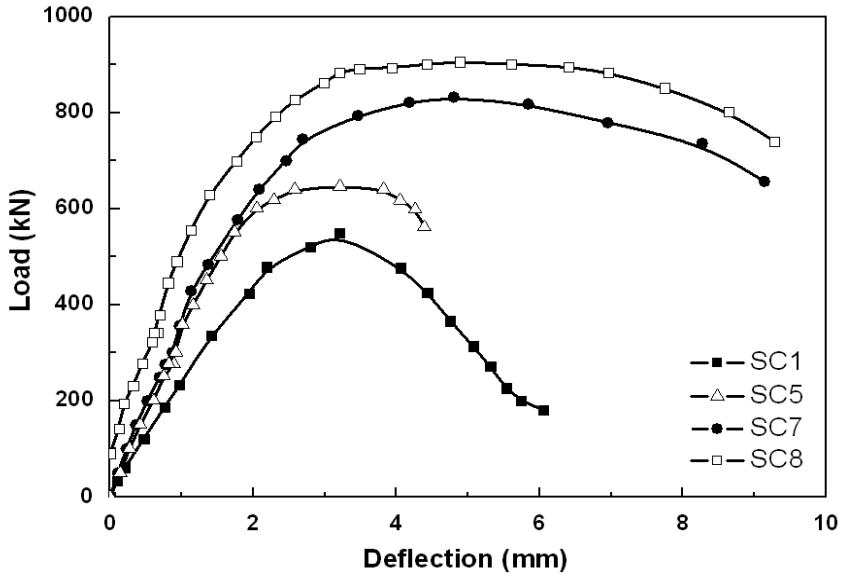

Figure 16 Load-deflection curves